






Article

Additive Manufacturing of Ceramic Reference Spheres by Stereolithography (SLA)

V́ctor Meana ¹, Pablo Zapico ¹, Eduardo Cuesta ^{1,*}, Sara Giganto ², Lorenzo Meana ¹
and Susana Mart́nez-Pellitero ²

¹ Department of Construction and Manufacturing Engineering, University of Oviedo, Campus of Gijon, 33203 Gijon, Spain; meanavictor@uniovi.es (V.M.); zapicopablo@uniovi.es (P.Z.); lorenzomeanaperez@gmail.com (L.M.)

² Area of Manufacturing Engineering, University of Leon—Universidad de Le3n, Campus of Vegazana, 24071 Leon, Spain; sgigf@unileon.es (S.G.); susana.martinez@unileon.es (S.M.-P.)

* Correspondence: ecuesta@uniovi.es

Abstract: Additive Manufacturing (AM) is advancing technologically towards the production of components for high-demand mechanical applications with stringent dimensional accuracy, leveraging metallic and ceramic raw materials. The AM process for ceramic components, known as Ultraviolet Laser Stereolithography (SLA), enables the fabrication of unique parts or small batches without substantial investments in molds and dies, and avoids the problems associated with traditional manufacturing, which involves multiple stages and final machining for precision. This study addresses the need to produce reference elements or targets for metrological applications, including verification, adjustment, or calibration of 3D scanners and mid- to high-range optical sensors. Precision spheres are a primary geometry in this context due to their straightforward mathematical definition, facilitating rapid and accurate error detection in equipment. Our objective is to exploit this novel SLA process along with the advantageous optical properties of technical ceramics (such as being white, matte, lightweight, and corrosion-resistant) to materialize these reference objects. Specifically, this work involves the fabrication of alumina hemispheres using SLA. The manufacturing process incorporates four design variables (wall thickness, support shape, fill type, and orientation) and one manufacturing variable (the arrangement of spheres on the printing tray). To evaluate the impact of the design variables, dimensional and geometric parameters (GD&T), including diameters, form errors, and their distribution on the surface of the sphere, have been characterized. These measurements are conducted with high accuracy using a Coordinate Measuring Machine (CMM). The study also examines the influence of these variables in the dimensional and geometric accuracy of the spheres. Correlations between various parameters were identified, specifically highlighting critical factors affecting process precision, such as the position of the piece on the print tray and the wall thickness value. The smallest diameter errors were recorded at the outermost positions of the tray (rear and front), while the smallest shape errors were found at the central position, in both cases with errors in the range of tens of micrometers. In any case, the smallest deformations were observed with the highest wall thickness (2 mm).

Keywords: additive manufacturing; stereolithography; ceramics; alumina; reference spheres



Citation: Meana, V.; Zapico, P.; Cuesta, E.; Giganto, S.; Meana, L.; Mart́nez-Pellitero, S. Additive Manufacturing of Ceramic Reference Spheres by Stereolithography (SLA). *Appl. Sci.* **2024**, *14*, 7530. <https://doi.org/10.3390/app14177530>

Academic Editors: Abhilash Puthanveetil Madathil and Xichun Luo

Received: 11 July 2024

Revised: 21 August 2024

Accepted: 22 August 2024

Published: 26 August 2024



Copyright: 2024 by the authors. Licensee MDPI, Basel, Switzerland. This article is an open access article distributed under the terms and conditions of the Creative Commons Attribution (CC BY) license (<https://creativecommons.org/licenses/by/4.0/>).

1. Introduction

The benefits of additive manufacturing (AM) compared to traditional manufacturing methods are widely acknowledged for its capacity to produce parts from various materials, intricate shapes, with great speed, enough precision, cost-effectiveness, and eliminating the need for fixtures and jigs [1–3]. These advantages are particularly significant when considering ceramic components, where their properties such as high melting temperatures, low ductility, and susceptibility to thermal shock, make conventional forming methods

expensive and difficult, often resulting in faulty parts, with defects and surface microcracks. But these issues, that have persisted for years in conventional methods, continue nowadays in additively manufactured ceramic parts due to the lack of on-site inspection and systematic procedures throughout the design, processing, and post-processing stages.

Among the various AM technologies for advanced ceramics, those based on photopolymerization stand out for producing parts with superior mechanical properties, high precision, and excellent surface finish [4]. Within this category, Vat Photopolymerization by Ultraviolet Laser for Ceramics technique (VPP-UVL/C according to ISO/ASTM 52900 [5]), commonly known as stereolithography (SLA), has shown promising results, particularly with materials like alumina, zirconia, and hydroxyapatite [6].

The SLA process for ceramics involves four critical stages in two phases: printing (production phase), cleaning, debinding, and sintering (post-processing phase). The raw material consists of a paste containing a suspension of ceramic particles in a photosensitive resin, along with diluents and binders. In the initial printing stage, a green (oversized) part is fabricated via photopolymerization, layer by layer, facilitated by ultraviolet light acting upon the photosensitive resins [7]. The paste is evenly distributed onto the printing bed using a blade that adjusts the layer height during each pass. Throughout this phase, layer displacements may occur, and microbubbles can form due to air entrapment during paste application [8]. The strategic use of supports is crucial to prevent structural failure resulting from the forces exerted during the process, which could lead to deformation, breakage of thin sections, or detachment of the part from the bed [9]. The stresses induced are contingent upon the rheological properties of the paste and the velocity and thickness of the layers, all relative to a given blade geometry.

The cleaning stage is critical, as the printed parts do not have sufficient consistency and are susceptible to breakage when the surrounding paste is removed. This involves removing all the ceramic paste that has not been photopolymerized and that not only surrounds the piece but is also stored in the hollows and interstices of the piece's geometry.

In the debinding stage, which constitutes the second phase, the removal of the organics of the photopolymerized resin is achieved through high temperature-time cycles. This process involves a combination of polymer evaporation, oxidation-induced decomposition, and thermal degradation. It stands as the most crucial stage, as any cracks or deformations occurring during debinding due to a significant reduction in the volume and, therefore, cannot be rectified in subsequent sintering phases. Initially, the evaporation of diluents creates an open porosity, facilitating the diffusion and subsequent evaporation of polymeric components undergoing pyrolysis. At the end of this stage, parts exhibit significant porosity, reaching up to 40%, resulting in a low mechanical strength of the parts [10].

In the fourth stage, known as sintering, the ceramic component devoid of resins undergoes exposure to high temperatures. During this phase, the porous structure is densified, fostering a robust bond among the ceramic particles. This densification invariably leads to volumetric contraction, ultimately resulting in the part attaining its intended design dimensions. Sintering conducted in ambient air typically yields material densities ranging from 95% to 99% of the theoretical maximum; however, sintering under vacuum or pressure conditions further reduces porosity levels. Studies have demonstrated that ceramic density and bending strength exhibit enhancement with increasing sintering temperature [11,12].

Alumina is a very versatile ceramic material, and its properties make it especially suitable for applications where temperature or biocompatibility are critical factors [13]. Due to its high hardness and stability, it serves as an abrasive, as a protective oxide on metal surfaces, as a refractory for furnaces and as a high-quality electrical insulator due to its high electrical resistance over a wide temperature range. Due to its excellent biocompatibility, it is used in biomedical applications. The white color, the dimensional stability with temperature, and the lightness of alumina has also aroused interest in the field of optical measuring equipment calibration [14], where reduction of weight for large-range master gauges and calibration devices makes the use of lightweight ceramics even more interesting [15].

Indeed, it is common to find research studies examining the metrological behaviors of ceramic reference elements, such as those made from alumina [16–18]. However, ceramic artifacts produced by conventional methods are solid and therefore heavy. Additionally, precision ceramic spheres typically have excellent dimensional qualities and surface finishes. They often use G5, G10 grades [19], which require very low roughness ($R_a < 0.02 \mu\text{m}$), resulting in shiny finishes that are unsuitable for use with many optical sensors (e.g., laser 3D scanners) [20]. To address this issue, it is beneficial to fabricate lightweight reference elements with high thermal stability and a matte finish that make them suitable for 3D scanners used in optical metrology and reverse engineering. The additive manufacturing processes for alumina spheres are promising candidates for producing these elements. This technique enables the creation of hollow, matte white spheres with relatively large diameters (up to 50 mm or more), reducing their weight and thus minimizing their impact on the deformation of the supporting structures, which is particularly advantageous for the calibration of medium- and high-range scanners.

However, there is a lack of research focused on this field using alumina parts fabricated through additive manufacturing processes involving ultraviolet laser photopolymerization. The chosen design for manufacturing the artifacts is based on a canonical sphere geometry, widely used as a reference element for equipment calibration. It is noteworthy that spheres represent a geometry that is straightforwardly definable in measurement software and ensures traceability of comparisons between measurements obtained by contact from a coordinate measuring machine (CMM).

In this work, artifacts based on hemispheres are designed and manufactured using four design variables (wall thickness, support shape, fill type, and orientation) and one manufacturing variable (arrangement of spheres on the printing tray) in order to analyze the influence of each on the achieved dimensional and geometric quality. For this purpose, diameters, shape errors, and the distribution of these errors on the surface of the spheres will be considered.

The following sections describe the equipment used for both the fabrication and measurement of the artifacts, the research methodology, the experimentation conducted, the results obtained, and the conclusions reached. Specifically, Section 2 is dedicated to presenting the equipment used and the methodology followed, from the initial step of proposing different designs to the final phase of analysis, including the fabrication of the parts and contact measurement using high-precision equipment. Section 3 details the experimentation, providing comprehensive information on the part designs, the parameters of the manufacturing stages, and the measurement processes. Section 4 presents the results of the geometric and dimensional parameter measurements. Finally, Section 5 enumerates the research conclusions based on the data analysis from the previous section.

2. Materials and Methodology

The work conducted in this experiment was carried out in four phases: design, manufacturing, measurement, and analysis. This sequence of operations is illustrated in Figure 1 and described in the following sections.

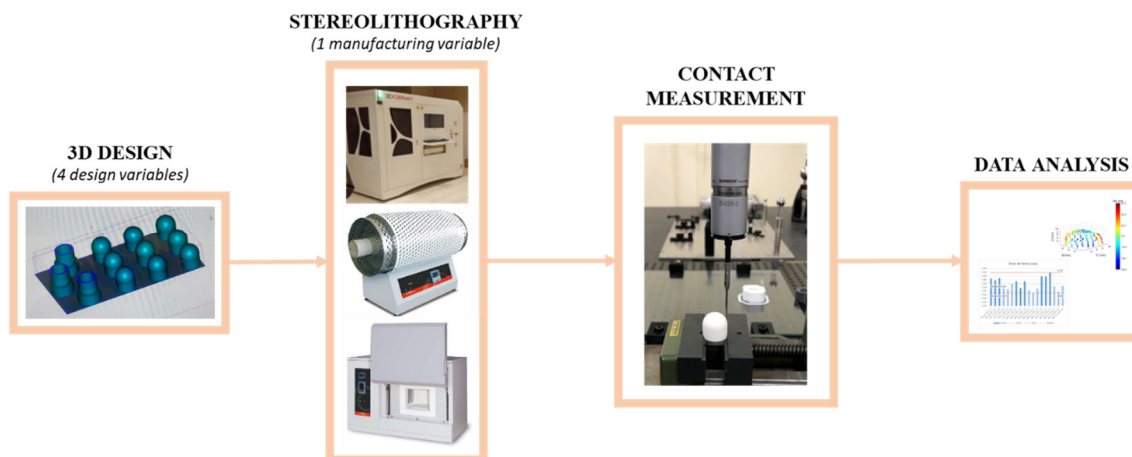


Figure 1. Methodology used for the experimentation.

2.1. Test Spheres Design

To achieve the objective of fabricating reference elements for 3D optical scanners, it is necessary to have some type of support that can be attached (usually by gluing) to the bottom of the spheres for securing them. Additionally, it is essential that the spheres have a well-defined diameter. Therefore, the solution involves manufacturing “extended hemispheres”, producing these elements from the pole to a “safety zone” below the equator, or vice versa (depending on the additive process strategy). Thus, starting from the CAD model of this extended hemisphere, different geometries of the master pattern have been designed, considering the manufacturer’s recommendations, as well as the limitations of the additive manufacturing process (SLA), mainly in the stages following printing (post-processing of the green part). According to the manufacturer’s recommendations, the maximum wall thicknesses should not exceed 5 mm, since deformations and cracks could appear during the removal of organics in the debinding stage. For this reason, and due to the search for lightweight structures that can be deployed as high and mid-range calibration and qualification standards, two wall thicknesses were used in the designed artifacts. As mentioned, the design of manufacturing’ supports are a crucial part of the design process, to avoid layer displacements during printing [21]. Different types of “set-up printing configurations” were considered. Figure 2 shows a 3D design of the layout of the test spheres on the printing tray. The colors represent different configurations of manufactured spheres which will be explained below (Section 3).

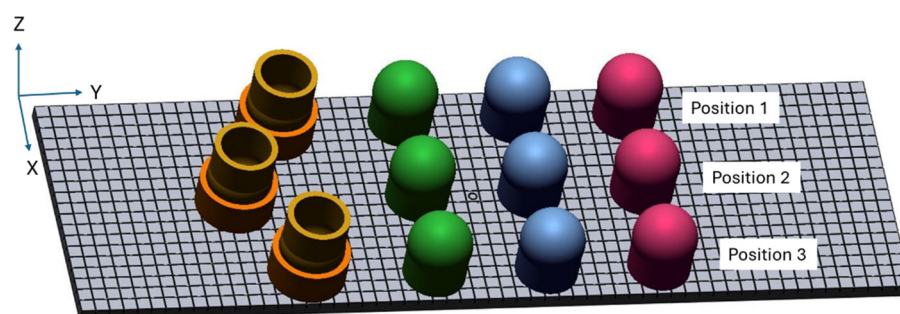


Figure 2. Layout of the CAD artifacts.

2.2. Additive Manufacturing by SLA

Once the different options to be evaluated were designed, the pieces were fabricated using stereolithography (SLA). As previously mentioned, this process involves several stages: printing, debinding, and sintering. There is also an intermediate cleaning process between the first and second stages. This cleaning is performed using a specific solution,

3DMIX Ceraclean (3DCeram, Bonnac-la-Côte, France), supplied by the manufacturer. The complete stereolithography system consists of the additive printer, a debinding furnace, and a sintering furnace.

The C900 Flex printer (3DCeram, Bonnac-la-Côte, France), Figure 3, has open parameters and is ideal for printing functional parts or small series, enabling the fabrication of ceramic parts by stereolithography with a maximum volume of $300 \times 300 \times 100$ mm, a layer thickness of $50 \mu\text{m}$, and a laser wavelength of 355 nm. The Ceradel PTF 16/130/610 (3DCeram, Bonnac-la-Côte, France) debinding furnace can reach a maximum temperature of $1300 \text{ }^\circ\text{C}$. The tube has a diameter of 130 mm, and the heated length is 500 mm. It features a manual adjustment for airflow and nitrogen to meet the heating requirements of the pieces. The sintering furnace is the HTL 20/17 (Thermoconcept, Bremen, Germany), with internal dimensions of $200 \times 250 \times 200$ mm and a power of 8 kW, capable of reaching a maximum temperature of $1750 \text{ }^\circ\text{C}$.

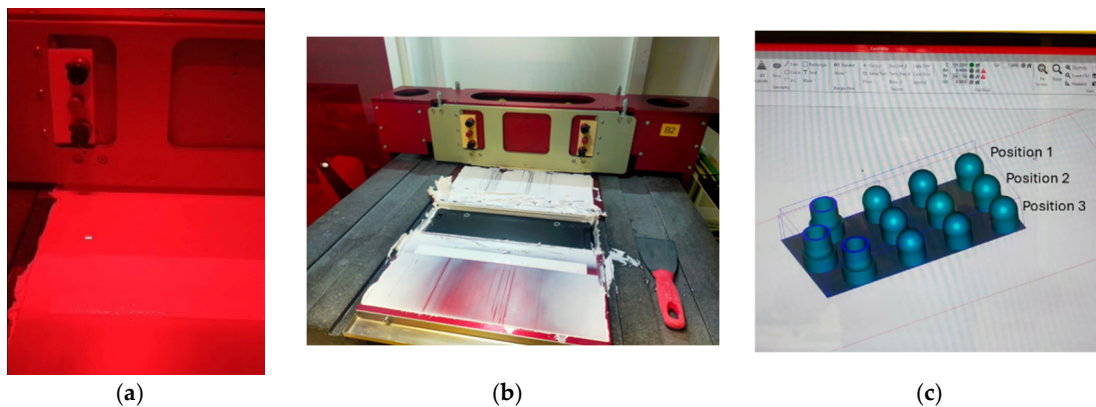


Figure 3. AM printer: (a) during the printing and light-curing process. (b) Printing tray after removal of the parts. (c) Spheres' layout on the AM machine display.

2.3. Measurement

The next step involved measuring the pieces using the Coordinate Measuring Machine (CMM), model DEA Global Image (Hexagon, Stockholm, Sweden). The machine was equipped with a PH10MQ indexing head (Renishaw, Gloucestershire, UK) and the probe used in this work was the SP25M (Renishaw, Gloucestershire, UK) with a tip of 40 mm long ceramic stylus with a $\text{Ø}4$ mm ruby sphere end. The accuracy of this CMM is given by the manufacturer according to ISO 10360-2 [22], Table 1.

Table 1. Coordinate Measuring Machine features.

Model	DEA Global Image 091508	
Measurement field	$900 \times 1500 \times 800$ mm	
Maximum permissible error	$2.2 + 0.003 L \mu\text{m}$ (L in mm)	
Maximum radial error	$2.2 \mu\text{m}$ (in repeatability)	
Maximum accuracy work Temp	$20 \pm 2 \text{ }^\circ\text{C}$	
Software	PC-DMIS, v2018 R2	

The inspection software controlling the machine is PC-DMIS 2018 R2. This equipment was used to carry out the measurements, providing reference values for the diameters and form errors of the spheres. To obtain these values, 100 contact points were recorded on each sphere, adhering to the criteria defined in ISO 10360-5 [23].

2.4. Analysis

Finally, the data obtained from the measurements conducted with the Coordinate Measuring Machine were analyzed. From this information, the diameter values and form errors were determined, which allowed for assessing the dimensional and geometric quality levels of the different spheres. Given the amount of data collected and the complexity of the variables involved, various scripts were developed using the Matlab programming platform to aid in data analysis and facilitate comparisons. A coding system was implemented to easily identify the structural characteristics of the manufactured models. The different graphical representations developed enabled the identification of correlations between variables from both dimensional and geometric analysis perspectives.

3. Experimentation

To carry out the experiment, a total of 24 pieces were manufactured (Table 2) in two different series, with 12 units in each. All the artifacts are spherical caps with a nominal diameter of 20 mm, each featuring different support geometries. These designs were intended to allow the artifacts to be placed on interchangeable supports for use as reference elements or targets in metrological applications.

Table 2. Artifacts manufactured according to the design variables.

		Artifacts Ø 20 mm			
		WT ¹ = 1 mm		WT ¹ = 2 mm	
		Mushroom ³	Bullet ³	Mushroom ³	Bullet ³
UP ²	Reticular filling (L)	-	-	3	-
	With inner support (F)	3	3	3	3
	Without inner support (E)	3	-	3	-
DOWN ²	Without inner support (E)	-	-	3	-

¹ Wall Thickness; ² Artifact orientation; ³ External geometry.

To enrich the study and enable an analysis of the influence of the manufacturing process, four design variables were considered:

- Vertical orientation (VO), which can be either Up (U) if the sphere has the pole up or Down (D) if the pole is down.
- Interior structure (IS), with three options: without internal support (E), with internal support (F), and with a lattice-type infill (L), see Figure 4. In the case of the solid support without contact, the gap part/support was 0.3 mm.
- External geometry of the artifact (EG), with two basic shapes considered: mushroom (M) and bullet (B). See Figure 5.
- Wall thickness (WT), either 1 or 2 mm.

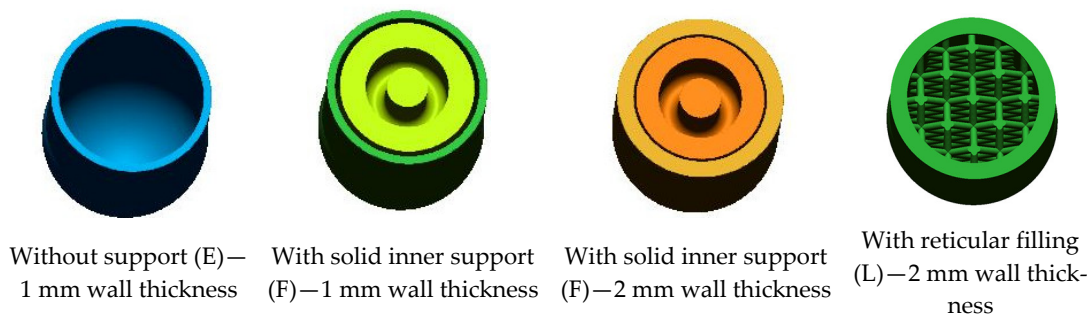


Figure 4. Different types of filling.

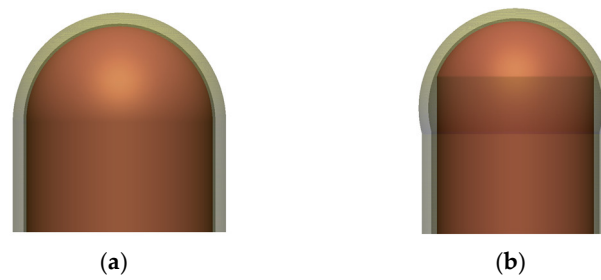


Figure 5. Different types of shape. (a) Bullet type with inner support. (b) Mushroom type with inner support.

There was one manufacturing variable:

- Position on the printing tray, rear (1), center (2), and front (3) (see Figures 2 and 3c).

Furthermore, thinking about the subsequent placement of the artifacts in another base device, the hemispheres were designed with two different shapes: Bullet type (B) (Figure 5a) and Mushroom type (M) (Figure 5b).

However, during the printing process of the first series, three units were discarded from the metrological analysis due to visible defects in the “green” state, the state before debinding (mushroom-type pieces without internal support, down position, and 2 mm wall thickness) (Figure 6a). Additionally, another three pieces (mushroom-type with lattice internal structure and 2 mm wall thickness) were discarded because they showed shape deviations greater than 0.3 mm after undergoing the complete process. These deformations were caused by the stresses produced by the lattice structure during the sintering phase (Figure 6b). Therefore, the subsequent metrological analysis considered only the remaining 18 artifacts.



Figure 6. (a) Mushroom-type artifacts, down orientation, E support and WT = 2 mm. (b) Mushroom-type artifact, Up orientation, L support and WT = 2 mm.

As previously mentioned, the printing process was carried out using Vat Photopolymerization by Ultraviolet Laser for Ceramics (VPP-UVL/C) in two series, each lasting approximately 18 h, using 3DMIX ALUMINA AL-F02 alumina paste supplied by the printer’s provider (3DCeram, Bonnac-la-Côte, France). This phase of the additive manufacturing process is the most sensitive regarding the potential to damage the pieces during handling, as the pieces do not yet have their final mechanical properties. In fact, once the print bed is removed from the printer, the pieces are not in sight (Figure 7a) as they are covered by the uncured ceramic paste, making their handling even more difficult. Cleaning to remove all traces of ceramic paste is meticulously carried out under an extraction hood (Figure 7b) to prevent the operator from inhaling gases emitted by the cleaning solution recommended by the manufacturer. This phase took 8 h, performed by a technician with specific training.

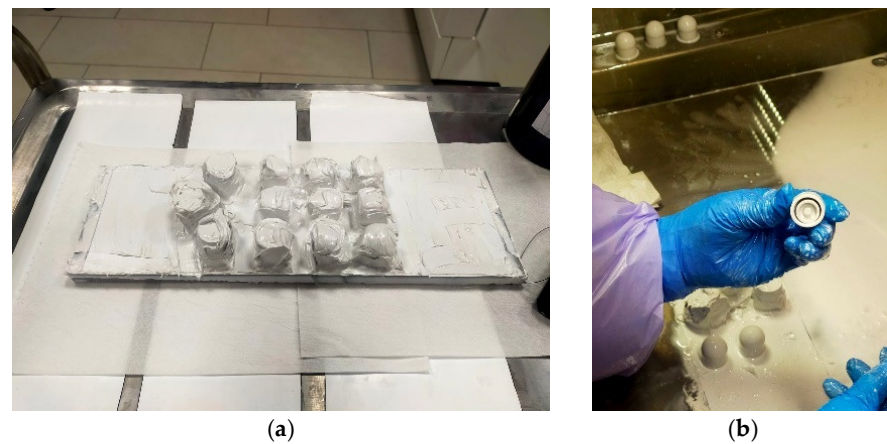


Figure 7. (a) Printing tray with parts filled with ceramic paste. (b) Cleaning of parts under the extraction hood.

The next phase in the artifact production process was debinding. This is a key step in the manufacturing process that consists of removing organics to leave only the ceramic matrix. The ceramic paste has a high binder content (40–60%) that must be eliminated by burning at high temperatures. During this stage, the resins are removed through a combination of evaporation of low molecular weight polymers, oxidative decomposition, and thermal degradation. The organic matrix burns off at temperatures up to 550 °C. In the initial phase, the diluent evaporates. As it does so, it creates open porosity within the green piece. This facilitates the diffusion and evaporation of the polymeric components that are subsequently pyrolyzed [24]. Table 3 shows the stages of the debinding process. Up to 800 °C it takes place with a constant nitrogen flow of 0.5 L/min. When 800 °C is reached, the progressive change from nitrogen to air is made. From 800 °C to the end of the process, it is carried out with a constant air flow of 0.5 L/min.

Table 3. Thermal stages in the debinding process.

	Environment	Temperature (°C)	Ramp (°C/min)	Stage (min)
1		20–240	0.2	1100
2		240	-	20
3	N ₂	240–460	0.1	2200
4		460	-	20
5		460–800	0.3	1133
6	N ₂ → Air	800	-	120
7		800–1050	1	250
8	Air	1050	-	5
9		1050–20	-2	515

In total, almost 4 days were required to complete this stage of the process, during which the thermal treatment was conducted in a nitrogen environment to achieve a smoother surface and higher density of the final pieces. Additionally, nitrogen was used to prevent porosity formation, thereby ensuring the quality and durability of the pieces. Figure 8 shows the debinding process with a time–temperature graph according to the parameters provided by the supplier of the raw material. This graph illustrates the different thermal stages, including the final heating to a maximum temperature of 1050 °C and subsequent cooling in an air environment.

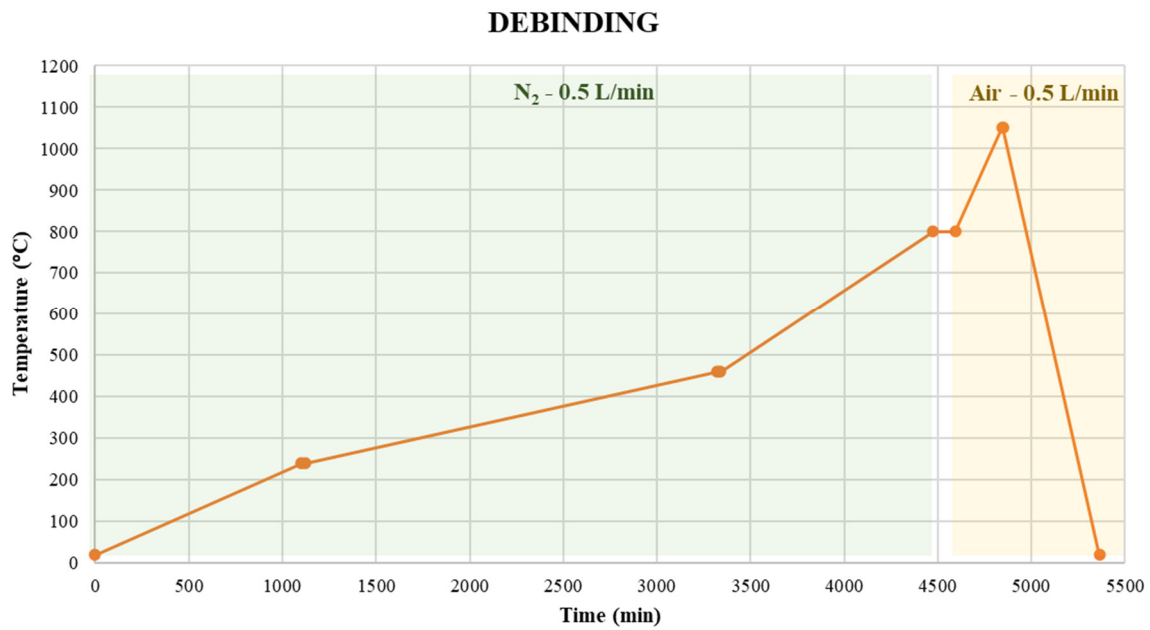
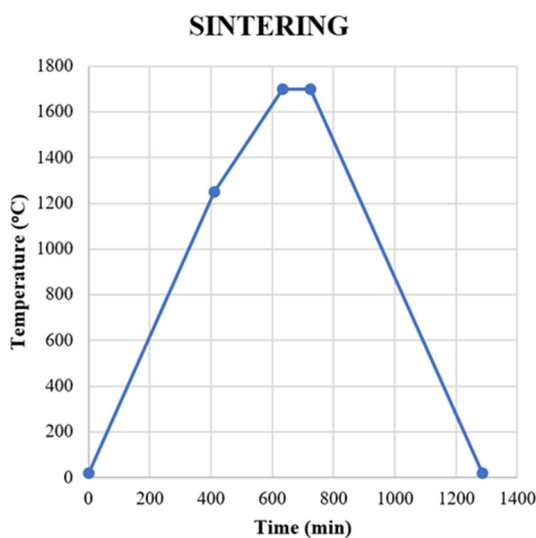


Figure 8. Thermal evolution in the debinding process.

Finally, the pieces underwent a new thermal treatment (air environment), this time for sintering. The goal of this stage was to achieve a dense and robust structure by eliminating porosities and providing the pieces with the necessary strength so that handling would not alter the designed dimensions and geometries. This research does not aim to achieve specific mechanical properties (strength, hardness, etc.), as previously mentioned. Instead, the intention is to utilize the material’s thermal stability and the lightweight design enabled by additive manufacturing to create metrological reference elements. According to the manufacturer’s specifications, this process involves reaching a maximum temperature of 1700 °C and lasts approximately 22 h, including both heating and cooling stages. Figure 9 shows the data and corresponding graph for the sintering process.



	Temperature (°C)	Ramp (°C/min)	Stage (min)
1	20–1250	3	410
2	1250–1700	2	225
3	1700	-	90
4	1700–20	−3	560

Figure 9. Sintering stage configuration and time vs. temperature diagram.

4. Results and Discussion

For the 18 spheres that were measured and analyzed, a nomenclature (Figure 10) was necessary to identify them according to their shape (B—bullet, M—mushroom), infill (ultimately only two types: F—with internal support, E—without internal support), orientation

(U—pole up, D—pole down), diameter in mm (20), wall thickness WT in mm (1, 2), and position on the tray (1, 2, 3).



Figure 10. Artifact nomenclature.

Additionally, to validate the process and conduct a metrological analysis that allowed for the evaluation of the influence of the proposed design variables, two parameters were evaluated: one dimensional (the diameter) and one geometric (the form error).

The results for the diameter values (Table 4) of the different spheres measured by contact with the CMM ranged from 20.033 mm, measured on the sphere M_E_U_20_2_1 (artifact with mushroom geometry, without internal support, oriented upwards, Ø20 mm, 2 mm wall thickness, in position 1 on the tray), to 19.916 mm, obtained on the sphere B_F_U_20_1_2 (artifact with bullet geometry, with internal support, oriented upwards, Ø20 mm, 1 mm wall thickness, in position 2 on the tray). Thus, the diameter range was 117 µm, with the average diameter of all spheres being only 9 µm below the nominal value (Figure 11).

Table 4. Diameters of the ceramic spheres manufactured by SLA.

Tray Location	Artifact Code (Bullet Shape, with Inner Support, Pole Upwards)	Diameter (mm)	Artifact Code (Mushroom Shape, without Inner Support, Pole Upwards)	Diameter (mm)	Artifact Code (Mushroom Shape, with Inner Support, Pole Upwards)	Diameter (mm)
Rear	B_F_U_20_1_1	20.018	M_E_U_20_1_1	20.059	M_F_U_20_1_1	20.029
Centre	B_F_U_20_1_2	19.903	M_E_U_20_1_2	19.980	M_F_U_20_1_2	19.917
Front	B_F_U_20_1_3	19.986	M_E_U_20_1_3	19.992	M_F_U_20_1_3	19.989
Rear	B_F_U_20_2_1	20.034	M_E_U_20_2_1	20.044	M_F_U_20_2_1	20.045
Centre	B_F_U_20_2_2	19.959	M_E_U_20_2_2	19.984	M_F_U_20_2_2	19.992
Front	B_F_U_20_2_3	20.010	M_E_U_20_2_3	20.033	M_F_U_20_2_3	20.048

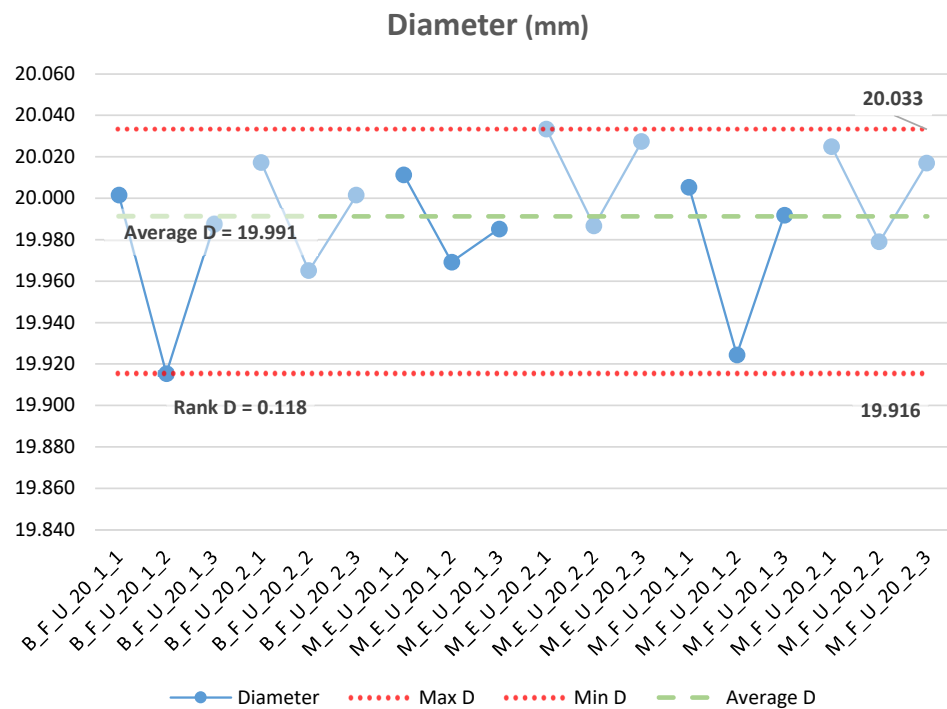


Figure 11. Dimensional quality chart of the different spheres.

Considering the arrangement of the different artifacts on the print tray, it can be observed that among the three possible positions, the intermediate position (position 2) always registers the smallest diameter values. It should also be noted that the values farthest from the nominal diameter, indicating the greatest contraction, correspond to the artifacts with the thinnest walls (1 mm) and internal support (B_F_U_20_1_2 and M_F_U_20_1_2). On the other hand, the average diameter of the spheres in position 3 deviates only 2 μm from the nominal diameter, with the values being closest to the nominal. Additionally, when examining the values corresponding to position 1, it is noted that in all cases, the values are always above the average diameter of all spheres (19.991 μm) and even above the nominal value. Regardless of the design variables and considering only the position on the print tray, it is significant to see the V-shaped distribution of all artifacts, which indicates the influence of the artifact's position.

Regarding geometric quality, the data obtained for the form error (Table 5) shows a behavior similar to that of the diameter. The intermediate position (position 2) records, for all artifacts, the smallest value among the three measured for each type of artifact (the same V-shaped distribution). In this case, the smallest value, 69 μm , was obtained for the artifact M_E_U_20_2_2 (artifact with mushroom geometry, without internal support, oriented upwards, $\text{\O}20$ mm, 2 mm wall thickness, and in position 2 on the tray), while the largest form error, 178 μm , was recorded for the artifact M_F_U_20_1_3 (artifact with mushroom geometry, with internal support, oriented upwards, $\text{\O}20$ mm, 2 mm wall thickness, and in position 1 on the tray). In this case, the range of form error measurements is 109 μm , while the average value of all form errors measured by contact is also slightly above one-tenth of a millimeter, 118 μm (Figure 12).

Table 5. Form errors of the spheres.

Tray Location	Artifact Code (Bullet Shape, with Inner Support, Pole Upwards)	Form Error (mm)	Artifact Code (Mushroom Shape, without Inner Support, Pole Upwards)	Form Error (mm)	Artifact Code (Mushroom Shape, with Inner Support, Pole Upwards)	Form Error (mm)
Rear	B_F_U_20_1_1	0.125	M_E_U_20_1_1	0.123	M_F_U_20_1_1	0.132
Center	B_F_U_20_1_2	0.096	M_E_U_20_1_2	0.075	M_F_U_20_1_2	0.112
Front	B_F_U_20_1_3	0.125	M_E_U_20_1_3	0.094	M_F_U_20_1_3	0.142
Rear	B_F_U_20_2_1	0.085	M_E_U_20_2_1	0.089	M_F_U_20_2_1	0.096
Center	B_F_U_20_2_2	0.077	M_E_U_20_2_2	0.075	M_F_U_20_2_2	0.071
Front	B_F_U_20_2_3	0.083	M_E_U_20_2_3	0.088	M_F_U_20_2_3	0.086

It is also observed that the highest geometric quality, with the smallest form errors, is recorded when the artifact walls are 2 mm thick, in both bullet (B) and mushroom (M) configurations. This clear dependency on wall thickness is even more pronounced when the artifact is manufactured without internal support, such that the model M_E_U_20_2_2 exhibits the smallest form error, as previously mentioned.

Additionally, analyzing the residuals obtained from the point clouds captured by contact with the SP25M (Renishaw, Gloucestershire, UK) on the 18 available spheres, it can be noted that all of them exhibit some ovalization error in the horizontal plane (OXY) and some flattening in the vertical direction (Z) across all possible combinations of design variables and positions. As an example, Figure 13 shows the magnified residuals of three evaluated artifacts.

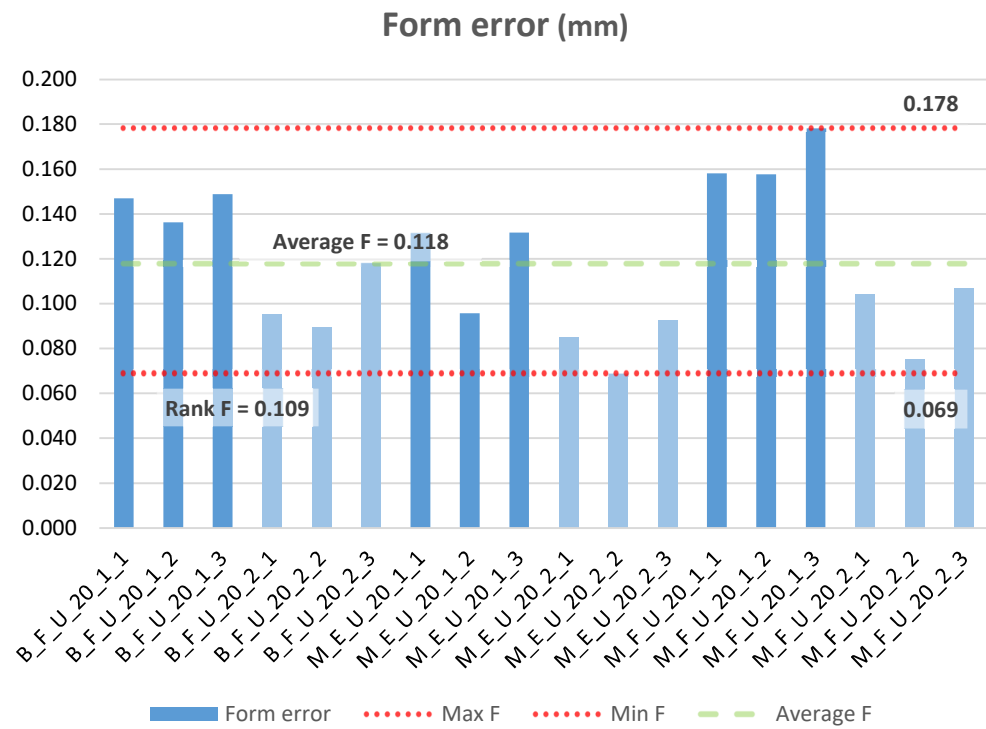


Figure 12. Geometrical quality chart of the different spheres.

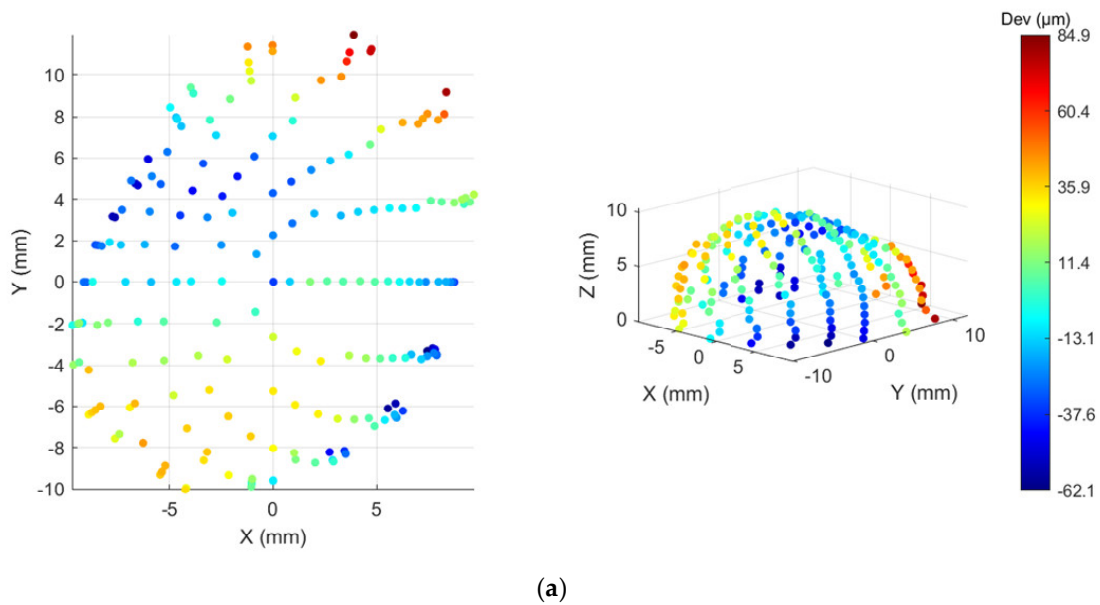


Figure 13. Cont.

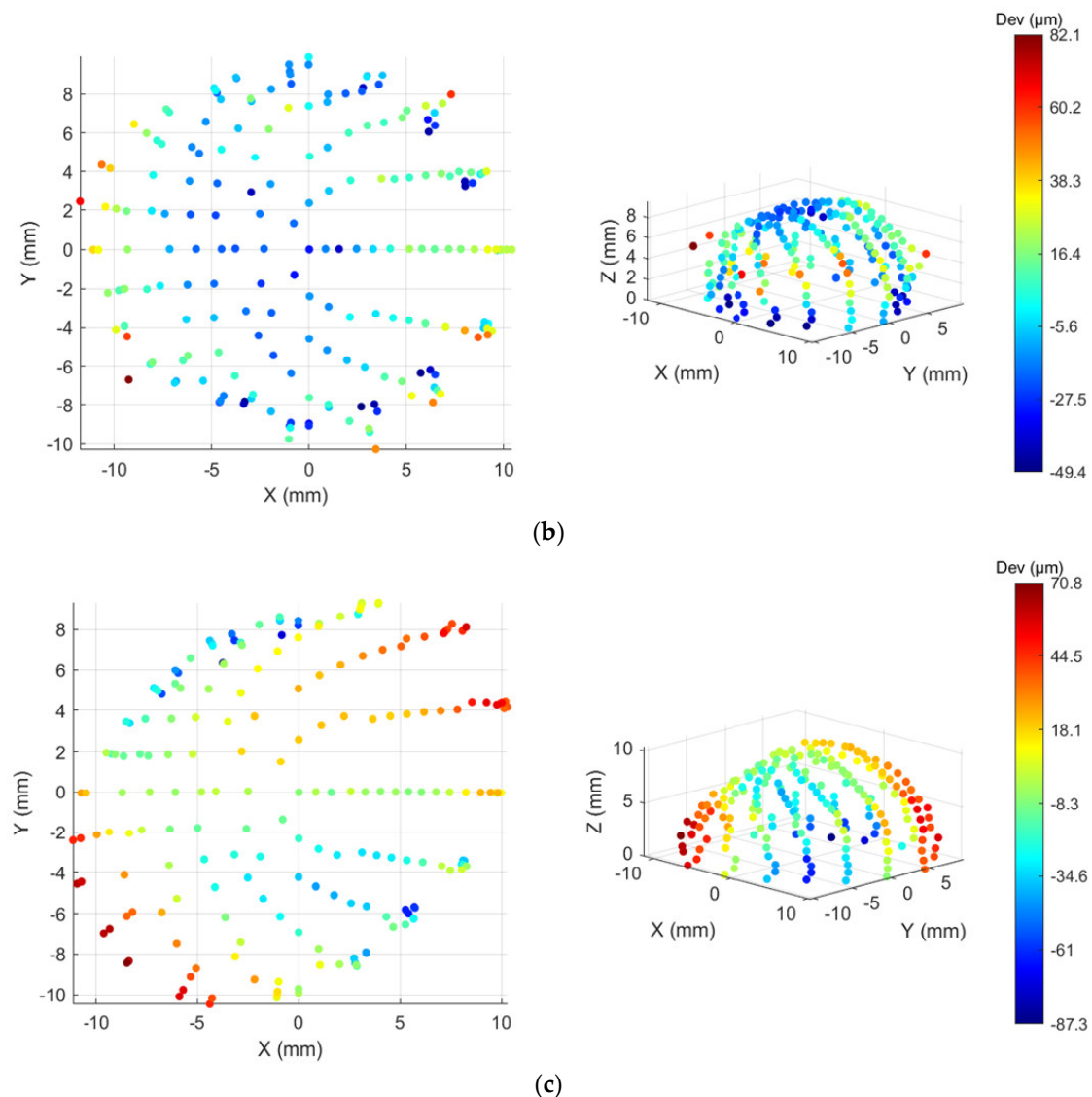


Figure 13. Examples of residuals with graphical magnification of deviations for different artifacts: (a) Bullet & Filled & Upwards B_F_U_20_1_1, (b) Mushroom & Empty & Upwards M_E_U_20_1_1 y (c) Mushroom & Filled & Upwards M_F_U_20_1_1.

Based on the above observations, it was decided to analyze the influence of process parameters on the quality indicators of the spheres, i.e., to determine whether using a sphere with different shape, infill, thickness, orientation, or position on the printing tray could yield a geometry closer to the nominal (with less diameter deviation and/or less form error). Ultimately, this analysis aimed to identify if a specific combination of design parameters could achieve a sphere with less deformation. The following correlations between design parameters and deviations (DesvD or DesvF) are highlighted from this analysis:

DesvD (Diameter Deviation): There is a correlation between the position in which the spheres are manufactured and the diameter deviation they exhibit. Spheres manufactured in positions 1 or 3 are better, followed by those made in position 2, which in all cases resulted in a smaller average size (Figure 14a).

DesvF (Form Error): (1) There is a correlation between wall thickness and observed form error, being smaller in spheres with a 2 mm thickness than in those with 1 mm (Figure 14b). (2) There is a correlation between infill and form error, with empty spheres (E) performing slightly better than filled ones (F) (Figure 14c). (3) There is some correlation,

though inconclusive, between position and form error, with the best spheres being those in position 2, followed by positions 1 and 3 (Figure 14d).

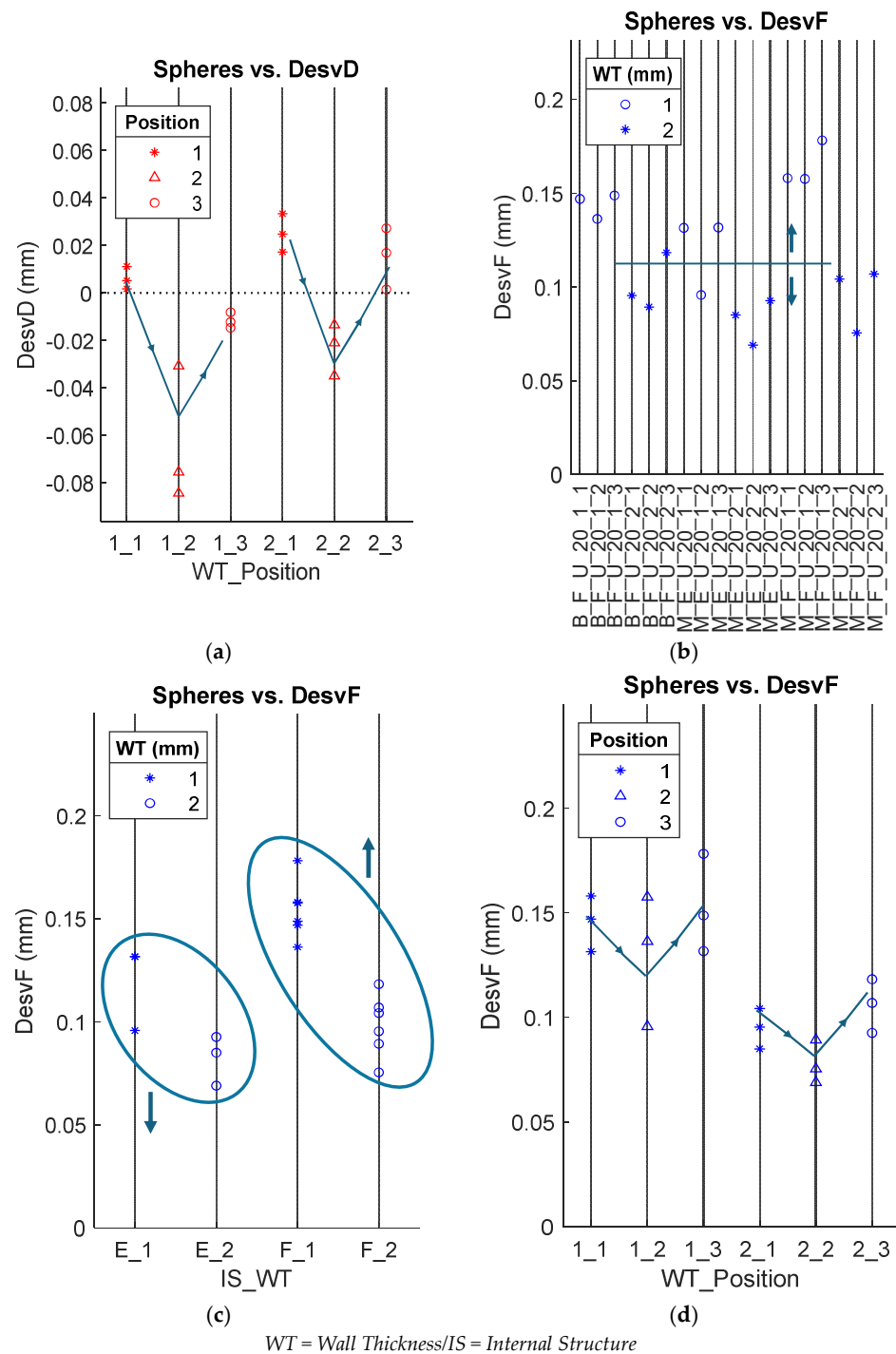


Figure 14. Different correlations between design variables and deviations of diameter and form error. (a) Correlation between the position and diameter deviations, (b) Correlation between wall thickness and form error deviations, (c) Correlation between infill and form error deviations, (d) Correlation between position and form error deviations.

5. Summary and Conclusions

This work analyses the influence of different design parameters on alumina parts obtained through additive manufacturing. The technology used was stereolithography (SLA) with an ultraviolet laser, and the fabricated parts were spheres with different supports and structures. These fabricated and analyzed artifacts could be used as reference elements or targets in metrological applications. The analysis also considered the position of the parts on the print tray. The influence of parameters (wall thickness, shape, infill, and orientation) was determined for the dimensional analysis of the spheres through the diameter and for the geometric analysis through the form error. The values of both characteristics were obtained by contact measurement of the spheres using a high-precision coordinate measuring machine (CMM). The entire manufacturing process (printing, cleaning, debinding, and sintering) was carried out according to the parameters specified by 3D Ceram, the supplier of the printing machine, the raw material, and the cleaning material.

The maximum deviations found in the diameter range between +33 μm and $-84 \mu\text{m}$, while the form error deviations range from 69 μm to 178 μm . Although the precision obtained in the diameter is on the order of hundredths and below two-tenths for the form error, these values are considered, a priori, too high for the spheres to be considered as reference elements in low-range metrology. It should be noted that the qualification/calibration spheres used in this range typically have much lower form errors, even submicrometric.

While all parts exhibit slight ovalization in the horizontal plane (OXY) and some flattening along the vertical axis (Z), with errors in the range of tens of micrometers, those positioned in positions 1 and 3 of the print tray (outer positions) show better results concerning the dimension (diameter). These parts not only exhibit less deviation from the nominal value but also show less dispersion in the values of the different spheres. Among these spheres, those fabricated with a 2 mm wall are the best quantitatively. On the other hand, the results indicate that the highest geometric quality of the spheres is achieved in those fabricated with a 2 mm wall, with an empty interior (no internal support) and, again, in position 2 of the print tray. It is clear that a thin wall (1 mm) is not sufficient to prevent deformation during the manufacturing process of alumina spheres via ultraviolet light stereolithography.

In any case, these observed deformations in the spheres could originate from two sources: machine errors and/or process errors. Probably, the deformations result from a combination of both, as the ovalization in the horizontal plane seems to be due to a squaring error of the X and Y axes, while the flattening in the vertical direction appears to be a linear error of the machine's Z axis, or a deformation caused in the material during the sintering process (flattening due to its own weight).

One of the most evident disadvantages observed during the experimentation is the high failure rate in manufacturing (25%) as well as the overall time required for production with this technology. However, these drawbacks are inherent to the process given the current state of development of this technology (ceramic parts manufactured via SLA).

As a summary, and based on the dimensional and geometric error results, it can be concluded that, as of now, the SLA process is not suitable for calibration artifacts in low-range and/or high-precision sensors. However, for medium- and long-range sensors and in the verification of master parts, this technology is viable, as deviations of less than 84 μm in diameter and 178 μm in form errors have been observed.

Future Works

Future studies could focus on validating the process for manufacturing alumina reference spheres which, when placed on supports made of lightweight and thermally stable materials, could be used to qualify medium- and high-range distance meters. There is a clear need to manufacture spheres of suitable sizes for various optical metrology equipment (3D scanners using photogrammetry, structured light, and/or laser profilometers), both portable (handheld models or integrated with AACMMs) and fixed (integrated with CMMs or robotic systems).

The technical feasibility of using ceramic materials as reference elements should be explored, considering their favorable properties such as being relatively lightweight, thermally stable, corrosion-resistant, and optically friendly (non-specular surfaces).

Nevertheless, the need to manufacture spheres of a size appropriate to their measurement field for various optical metrology equipment, both portable and fixed is evident.

In fact, as future work, the production of these elements in larger diameters, up to 50 mm (the limit of the available printing machine's capacity), is planned. This new range of diameters will be particularly important for the verification of medium- and high-range sensors.

Additionally, there is an intention to compare the manufacturing of these ceramic reference elements with other additive manufacturing technologies different from the SLA used in this research, such as Direct Light Processing (DLP) technology.

Author Contributions: Conceptualization, V.M. and P.Z.; methodology, V.M. and E.C.; validation, P.Z., S.G. and L.M.; writing—original draft preparation, V.M.; writing—review and editing, E.C., P.Z., S.G. and L.M.; visualization, S.G. and L.M.; supervision, E.C., P.Z. and S.M.-P.; project administration, V.M. and S.M.-P. All authors have read and agreed to the published version of the manuscript.

Funding: This research was funded by University Institute of Industrial Technology of Asturias (IUTA), grant number SV-23-GIJON-1-01 and also by MICIU/AEI/10.13039/501100011033 and, as appropriate, by “ERDF A way of making Europe”, by “ERDF/EU”, by the European Union; grant number PID2021-125992OB-I00.

Institutional Review Board Statement: Not applicable.

Informed Consent Statement: Not applicable.

Data Availability Statement: The raw data supporting the conclusions of this article will be made available by the authors on request.

Conflicts of Interest: The authors declare that they have no known competing financial interests or personal relationships that could have appeared to influence the work reported in this paper.

References

1. Chadha, U.; Abrol, A.; Vora, N.P.; Tiwari, A.; Shanker, S.K.; Selvaraj, S.K. Performance evaluation of 3D printing technologies: A review, recent advances, current challenges, and future directions. *Prog. Addit. Manuf.* **2022**, *7*, 853–886. [\[CrossRef\]](#)
2. Dilberoglu, U.M.; Gharehpapagh, B.; Yaman, U.; Dolen, M. The Role of Additive Manufacturing in the Era of Industry 4.0. *Procedia Manuf.* **2017**, *11*, 545–554. [\[CrossRef\]](#)
3. Shahrubudin, N.; Lee, T.C.; Ramlan, R.J.P.M. An overview on 3D printing technology: Technological, materials, and applications. *Procedia Manuf.* **2019**, *35*, 1286–1296. [\[CrossRef\]](#)
4. Bove, A.; Calignano, F.; Galati, M.; Iuliano, L. Photopolymerization of Ceramic Resins by Stereolithography Process: A Review. *Appl. Sci.* **2022**, *12*, 3591. [\[CrossRef\]](#)
5. *ISO/ASTM 52900:2021; Additive Manufacturing—General Principles—Fundamentals and Vocabulary*. International Organization for Standardization (ISO): Geneva, Switzerland, 2021.
6. Kushwaha, A.K.; Rahman, M.H.; Hart, D.; Hughes, B.; Saldana, D.A.; Zollars, C.; Rajak, D.K.; Menezes, P.L. 3-Fundamentals of stereolithography: Techniques, properties, and applications. *Tribol. Addit. Manuf. Mater.* **2022**, *87*–106.
7. Riccio, C.; Civera, M.; Grimaldo Ruiz, O.; Pedullà, P.; Rodriguez Reinoso, M.; Tommasi, G.; Vollaro, M.; Surace, C. Effects of Curing on Photosensitive Resins in SLA Additive Manufacturing. *Appl. Mech.* **2021**, *2*, 942–955. [\[CrossRef\]](#)
8. Zhang, G.; Zou, B.; Wang, X.; Yu, Y.; Chen, Q. Design, manufacturing and properties of controllable porosity of ceramic filters based on SLA-3D printing technology. *Ceram. Int.* **2023**, *49*, 1009–1019. [\[CrossRef\]](#)
9. Pateloup, V.; Michaud, P.; Chartier, T. Optimization of part orientation and adapted supports for manufacturing of ceramic parts by stereolithography using finite element simulations. *Open Ceram.* **2021**, *6*, 100132. [\[CrossRef\]](#)
10. Li, H.; Liu, Y.; Liu, Y.; Hu, K.; Lu, Z.; Liang, J. Investigating the relation between debinding atmosphere and mechanical properties of stereolithography-based three-dimensional printed Al₂O₃ ceramic. *Proc. Inst. Mech. Eng. B J. Eng. Manuf.* **2020**, *234*, 1686–1694. [\[CrossRef\]](#)
11. Li, H.; Liu, Y.; Colombo, P.; Li, W.; Liu, Y.; Hu, K.; Lu, Z. The influence of sintering procedure and porosity on the properties of 3D printed alumina ceramic cores. *Ceram. Int.* **2021**, *47*, 27668–27676. [\[CrossRef\]](#)
12. Li, H.; Liu, Y.; Li, W.; Liu, Y.; Zeng, Q. The effect of sintering on the properties of calcium oxide promoted alumina-based ceramic cores via 3D printing. *Mater. Chem. Phys.* **2021**, *263*, 124443. [\[CrossRef\]](#)

13. Melchels, F.P.; Feijen, J.; Grijpma, D.W. A review on stereolithography and its applications in biomedical engineering. *Biomaterials* **2010**, *31*, 6121–6130. [[CrossRef](#)] [[PubMed](#)]
14. Cuesta, E.; Alvarez, B.J.; Martinez-Pellitero, S.; Barreiro, J.; Patiño, H. Metrological evaluation of laser scanner integrated with measuring arm using optical feature-based gauge. *Opt. Lasers Eng.* **2019**, *121*, 120–132. [[CrossRef](#)]
15. Carmignato, S.; De Chiffre, L.; Bosse, H.; Leach, R.K.; Balsamo, A.; Estler, W.T. Dimensional artefacts to achieve metrological traceability in advanced manufacturing. *CIRP Ann. Manuf. Technol.* **2020**, *69*, 693–716. [[CrossRef](#)]
16. Zapico, P.; Meana, V.; Cuesta, E.; Mateos, S. Optical Characterization of Materials for Precision Reference Spheres for Use with Structured Light Sensors. *Materials* **2023**, *16*, 5443. [[CrossRef](#)] [[PubMed](#)]
17. Harmatys, W.; Gaska, P.; Gaska, A.; Gruza, M.; Jedynak, M.; Kobiela, K.; Marxer, M. Applicability Assessment of Different Materials for Standards Ensuring Comparability of Optical and Tactile Coordinate Measurements. *Materials* **2022**, *15*, 4128. [[CrossRef](#)] [[PubMed](#)]
18. Cai, Y.; Xie, B.; Ling, S.; Fan, K.C. On-Line Measurement Method for Diameter and Roundness Error of Balls. *Nanomanuf. Metrol.* **2020**, *3*, 218–227. [[CrossRef](#)]
19. *DIN 5401: 2002-08; Rolling Bearings—Balls for Rolling Bearings and General Industrial Use*. DIN: Berlin, Germany, 2002.
20. Meana, V.; Cuesta, E.; Álvarez, B.J. Testing the Sandblasting Process in the Manufacturing of Reference Spheres for Non-Contact Metrology Applications. *Materials* **2021**, *14*, 5187. [[CrossRef](#)] [[PubMed](#)]
21. Martínez-Pellitero, S.; Souto, A.M.; Peláez Peláez, S.; Barreiro García, J.; Castro Sastre, M.Á. Design of supports to avoid deformations in the process of alumina printing by stereolithography. *Key Eng. Mat.* **2023**, *958*, 67–75. [[CrossRef](#)]
22. *ISO 10360-2:2009; Geometrical Product Specifications (GPS)—Acceptance and Reverification Tests for Coordinate Measuring Machines (CMM): Part 2: CMMs Used for Measuring Linear dimensions*. International Organization for Standardization (ISO): Geneva, Switzerland, 2009.
23. *ISO 10360-5:2010; Geometrical Product Specifications (GPS)—Acceptance and Reverification Tests for Coordinate Measuring Systems (CMS)—Part 5: Coordinate Measuring Machines (CMMs) Using Single and Multiple Stylus Contacting Probing Systems Using Discrete Point and/or Scanning Measuring Mode*. International Organization for Standardization (ISO): Geneva, Switzerland, 2010.
24. Pfaffinger, M.; Mitteramskogler, G.; Gmeiner, R.; Stampfl, J. Thermal Debinding of Ceramic-Filled Photopolymers. *Mater. Sci. Forum* **2015**, *825*, 75–81. [[CrossRef](#)]

Disclaimer/Publisher’s Note: The statements, opinions and data contained in all publications are solely those of the individual author(s) and contributor(s) and not of MDPI and/or the editor(s). MDPI and/or the editor(s) disclaim responsibility for any injury to people or property resulting from any ideas, methods, instructions or products referred to in the content.